

SWORD: Spectral Wasserstein Online Regime Detection in Dynamic Networks

Izhar Ali
Department of Computer Science
Rowan University
aliizh94@rowan.edu

Abstract

Online change point detection in dynamic graphs requires comparing graphs as they arrive, in time linear in the number of edges, without parametric assumptions. Recent spectral methods address scale via the Kernel Polynomial Method (KPM): SCPD computes Chebyshev moments of the normalized Laplacian, discretizes them into a density-of-states histogram, and scores the histogram with SVD plus cosine similarity. We introduce SWORD, which computes the same moments and instead compares their mean across two adjacent time windows by their L_1 distance. On three real-world benchmarks (MIT Reality, AskUbuntu, Enron), this lifts mean F_1 from SCPD’s 0.27 to 0.79, with SCPD failing to detect any change on Enron. A controlled cascading ablation attributes the gap to two design choices: the two-window mean structure (dominant on MIT) and the L_1 metric on those mean vectors (dominant on Enron). A bin-width sweep rules out histogram discretization—SCPD’s most visible architectural choice—as the driver. SWORD inherits SCPD’s KPM core, so per-graph cost is $O(KRm)$ with no eigendecomposition, scaling to 86,000-node networks. With per-dataset tuning it matches the offline TIRE autoencoder on mean F_1 and attains the highest precision among online methods (0.91, only 2 false positives across the three benchmarks).

1 Introduction

Dynamic networks undergo structural transitions that signal important events: a corporate reorganization reshapes email communication (Peel and Clauset, 2015), a product launch restructures Q&A activity, or a disease outbreak alters contact patterns (Ideker and Krogan, 2012). Online *change point detection* (CPD) flags these transitions as the graph stream arrives and imposes four constraints: (i) decisions use only past observations; (ii) detection delay must be small while false alarms stay controlled; (iii) no parametric assumption on the graph-generating process; (iv) computation scales to graphs with $n \sim 10^5$ nodes. We still benchmark against retrospective and $O(n^3)$ spectral baselines for completeness.

Existing approaches each sacrifice something. *Feature-based methods* (CUSUM (Page, 1954), EWMA (Roberts, 1959)) collapse graph structure into scalars like mean degree, missing reorganizations that leave aggregates unchanged. *Kernel methods* like MMD (Gretton et al., 2012) capture distributional differences but require kernel and bandwidth choices that themselves affect sensitivity. *Spectral methods* encode global structure through eigenvalues: LAD (Huang et al., 2020) compares Laplacian singular values directly but relies on $O(n^3)$ eigendecomposition; SCPD (Huang et al., 2023) avoids eigendecomposition via KPM but discretizes the resulting moments into a density-of-states histogram and scores them with SVD-based cosine similarity.

This paper makes two contributions:

1. SCPD and SWORD share KPM moment computation, so the gap must lie in how the moments are compared. A cascading ablation (Figure 2) attributes it to two design choices: averaging moment vectors across two adjacent time windows (dominant on MIT), and using L_1 rather than cosine similarity on those means (dominant on Enron). Histogram discretization—SCPD’s most visible architectural choice—does not explain the gap: a bin-width sweep (Figure 3) leaves F_1 essentially flat.
2. SWORD takes the L_1 distance between Chebyshev moments of two sliding windows; KPM keeps per-graph cost at $O(KRm)$, linear in edges, and scales to 86,000-node networks. Windows can be symmetric, asymmetric, or exponentially weighted. Empirically $k = 2\text{--}4$ moments suffice, with F_1 degrading past $k \approx 5$ on MIT and Enron and plateauing on AskUbuntu (Section J).

2 Related Work

The survey of Mei et al. (2025) catalogs the field of graph CPD. We organize the literature into three families: statistical summaries, direct graph distances, and learned representations.

Statistical approaches reduce each graph to a summary and apply a classical test. Peel and Clauset (2015) fit hierarchical random graph models with Bayesian testing; Enikeeva and Klopp (2025) apply matrix-CUSUM to adjacency statistics; Ho et al. (2025) give martingale-based guarantees; Kei et al. (2025) fit a separable STERGM and detect via ADMM with a generalized fused lasso. These methods offer strong theory but compress graphs into low-dimensional summaries or parametric fits, which can miss higher-order spectral changes.

Distance-based approaches compare graphs directly. DeltaCon (Koutra et al., 2016) uses linearized belief propagation; LAD (Huang et al., 2020) compares Laplacian singular values across short and long windows; NetLSD (Tsitsulin et al., 2018) compares heat-trace signatures. All three rely on $O(n^3)$ matrix operations and do not scale to graphs with $\sim 10^5$ nodes.

Learned representations avoid hand-crafted features. The TIRE autoencoder (De Ryck et al., 2021) is the strongest unsupervised example, though it processes the full sequence; we benchmark it as a representative learned baseline.

The Kernel Polynomial Method (KPM; Weiße et al., 2006; Lin et al., 2016) avoids eigendecomposition by approximating spectral functions via Chebyshev expansion. Combined with Hutchinson’s stochastic trace estimator (Hutchinson, 1990), KPM computes spectral moments in $O(KRm)$ time, where K is the number of moments, R the number of random probes, and m the number of edges. Braverman et al. (2022) and Musco et al. (2025) proved that matching k Chebyshev moments approximates the Wasserstein distance with $O(1/k)$ error; Musco and Musco (2025) sharpens the underlying spectral density estimation via deflation. The network density of states (DOS) was introduced by Dong et al. (2019) as a scalable spectral summary, and LAddos (Huang et al., 2021) applied DOS histograms to CPD. SCPD (Huang et al., 2023) extended LAddos with attributed local DOS.

SCPD is the closest prior work; SWORD inherits its KPM moment computation but diverges on (i) scoring—SCPD bins moments into a DOS histogram and scores with SVD-based cosine plus a first difference, while SWORD applies a two-window L_1 comparison directly to the moment vectors—and (ii) windowing: SWORD adds asymmetric and exponentially weighted variants that reduce detection delay. To our knowledge, SWORD is the first method to use Chebyshev–Wasserstein moment matching as an online detection statistic for dynamic networks.

3 Problem Formulation

We observe a sequence of undirected graphs $\{G_t\}_{t \geq 1}$, where $G_t = (V_t, E_t)$ has n_t nodes and adjacency matrix $A_t \in \{0, 1\}^{n_t \times n_t}$. The task is to flag a change in the underlying generative process as soon as possible after it occurs while controlling false alarms.

Definition 3.1 (Online Change Point Detection). Under H_0 , all G_t are drawn i.i.d. from P_0 . Under H_1 , there exists $\tau^* \geq 1$ such that $G_t \sim P_0$ for $t < \tau^*$ and $G_t \sim P_1 \neq P_0$ for $t \geq \tau^*$. A detection rule is a stopping time τ adapted to $\mathcal{F}_t = \sigma(G_1, \dots, G_t)$.

Multiple change points are handled by restarting the rule after each detection (Lorden, 1971).

4 Method: SWORD

4.1 Spectral Measures and Wasserstein Distance

Scalar summaries like edge count cannot distinguish a clustered network from a random one of identical density, whereas the Laplacian spectrum encodes connectedness via λ_2 and community count via the near-zero eigenvalues (Gu et al., 2015). A distance between eigenvalue distributions is therefore a natural detection statistic.

For a graph G with n nodes, let $L = I - D^{-1/2}AD^{-1/2}$ denote the normalized Laplacian (eigenvalues in $[0, 2]$). Its *spectral measure* is the empirical eigenvalue distribution $\mu_G = \frac{1}{n} \sum_{i=1}^n \delta_{\lambda_i}$, where δ_{λ_i} is unit mass at λ_i . We compare spectral measures via the 1-Wasserstein distance W_1 , which on \mathbb{R} admits the closed form

$$W_1(\mu_{G_t}, \mu_{G_{t+1}}) = \frac{1}{n} \sum_{i=1}^n |\lambda_i^{(t)} - \lambda_i^{(t+1)}| \quad (1)$$

on sorted eigenvalues—parameter-free and geometrically natural, but $O(n^3)$ to compute.

4.2 Chebyshev Moments and Wasserstein Approximation

Rather than computing all n eigenvalues, we approximate W_1 via Chebyshev moments. By Kantorovich–Rubinstein duality, W_1 equals a supremum over 1-Lipschitz test functions, and Chebyshev polynomials approximate this class efficiently on $[-1, 1]$.

Shifting the spectrum via $\tilde{L} = L - I$ maps eigenvalues from $[0, 2]$ to $[-1, 1]$. The k -th Chebyshev moment is

$$\mu_k(G) = \frac{1}{n} \text{tr}(T_k(\tilde{L})), \quad (2)$$

with T_k the k -th Chebyshev polynomial of the first kind; $\mu_0 = 1$, $\mu_1 = 0$, and μ_2 measures eigenvalue spread. We measure spectral difference via the L_1 moment distance

$$d_k(G, G') = \sum_{j=1}^k |\mu_j(G) - \mu_j(G')| \quad (3)$$

(excluding $j = 0$, which is fixed by normalization).

Theorem 4.1 (Moment distance bounds Wasserstein; Musco et al., 2025, Thm. 1). *Let μ, ν be probability measures on $[-1, 1]$ with Chebyshev moments μ_j, ν_j , and let $\Gamma^2 = \sum_{j=1}^k (\mu_j - \nu_j)^2 / j^2$. Then $W_1(\mu, \nu) \leq C/k + \Gamma$ with $C \leq 36$ a universal constant.*

Since $1/j^2 \leq 1$ and $\|\cdot\|_2 \leq \|\cdot\|_1$, the unweighted d_k dominates Γ , so $W_1 \leq C/k + d_k$ holds too.

The bound monotonically tightens in k but does not predict an optimum: estimating μ_k stochastically (§4.3) adds variance that compounds with k , and the two effects balance empirically at $k = 2\text{--}4$ moments (Section J). For practical $k = 2\text{--}7$, C/k exceeds $W_1^{\max}=2$ on a normalized spectrum, so the theorem motivates moment matching rather than guaranteeing accuracy at the k we use (Limitation 2).

4.3 Scalable Computation via KPM

Forming $T_k(\tilde{L})$ explicitly is $O(n^3)$. Two matrix-free tricks reduce this to $O(m)$ per moment. First, Hutchinson’s estimator (Hutchinson, 1990) replaces the trace by $\text{tr}(M) = \mathbb{E}[z^\top M z]$ for Rademacher $z \in \{-1, +1\}^n$, averaged over R probes:

$$\hat{\mu}_k = \frac{1}{nR} \sum_{r=1}^R z_r^\top T_k(\tilde{L}) z_r. \quad (4)$$

Second, the Chebyshev recurrence $T_{k+1}(x) = 2xT_k(x) - T_{k-1}(x)$ lets us evaluate $v_k = T_k(\tilde{L})z$ iteratively:

$$v_0 = z, \quad v_1 = \tilde{L}z, \quad v_{k+1} = 2\tilde{L}v_k - v_{k-1}, \quad (5)$$

storing only the two most recent vectors. Each step is one sparse matvec, so K moments with R probes cost $O(KRm)$ per graph—linear in edges. The estimator is unbiased with $O(1/\sqrt{nR})$ per-moment standard deviation (because $\|T_k(\tilde{L})\|_F = O(\sqrt{n})$ for normalized Laplacians). We fix $K = 50$ and $R = 30$ and tune $k \leq 8$ for detection without recomputation.

4.4 Two-Window Comparison

For each graph G_t , let $\boldsymbol{\mu}(G_t) = [\mu_1(G_t), \dots, \mu_k(G_t)]^\top$ denote its moment vector (excluding $\mu_0 = 1$). At each time step t , we collect the w most recent graphs into a *test window* and the w_{ref} graphs immediately before it into a *reference window*:

Definition 4.2 (Two-Window Statistic). The test window $\mathcal{W}_{\text{test}} = \{t-w+1, \dots, t\}$ contains the w most recent graphs. The reference window $\mathcal{W}_{\text{ref}} = \{t-w-w_{\text{ref}}+1, \dots, t-w\}$ contains the w_{ref} graphs immediately preceding it. Let $\bar{\boldsymbol{\mu}}_{\text{test}} = \sum_{i \in \mathcal{W}_{\text{test}}} \alpha_i \boldsymbol{\mu}(G_i)$ and $\bar{\boldsymbol{\mu}}_{\text{ref}} = \sum_{j \in \mathcal{W}_{\text{ref}}} \beta_j \boldsymbol{\mu}(G_j)$ denote the window-mean moment vectors, where $\{\alpha_i\}, \{\beta_j\}$ are normalized weight vectors over each window. We consider three aggregation forms, all measuring discrepancy between the two windows:

$$D_t^{\text{pw}} = \sum_{i \in \mathcal{W}_{\text{test}}} \sum_{j \in \mathcal{W}_{\text{ref}}} \alpha_i \beta_j d_k(G_i, G_j) \quad (\text{mean-pairwise; default}) \quad (6)$$

$$D_t^{\text{cen}} = \|\bar{\boldsymbol{\mu}}_{\text{test}} - \bar{\boldsymbol{\mu}}_{\text{ref}}\|_1 \quad (\text{centroid-}L_1) \quad (7)$$

$$D_t^\Gamma = \left(\sum_{j=1}^k \frac{(\bar{\mu}_j^{\text{test}} - \bar{\mu}_j^{\text{ref}})^2}{j^2} \right)^{1/2} \quad (\text{weighted-}\Gamma) \quad (8)$$

The mean-pairwise form is the default; all three are searched in the grid (Section E). We write D_t when the mode is unspecified.

Symmetric windows take $w_{\text{ref}} = w$ with uniform weights. *Asymmetric windows* ($w_{\text{ref}} > w$) pair a short test window for fast response with a longer reference for a stable baseline, cutting detection delay to about w steps. Exponential weighting emphasizes recent observations in each window.

Under linear drift with stationary residuals ($\mathbb{E}[\mu_k(G_t)] = \mu_k^{(0)} + t\beta_k$), $\mathbb{E}[D_t]$ is t -independent for all three aggregation forms: centroid- L_1 and weighted- Γ depend on $\mathbb{E}[\bar{\mu}_{\text{test}} - \bar{\mu}_{\text{ref}}] = \frac{w+w_{\text{ref}}}{2}\beta$, and the expected lag between mean-pairwise indices is also $\frac{w+w_{\text{ref}}}{2}$, so $\mathbb{E}[|x_i - y_j|]$ is t -independent too. A fixed threshold therefore survives long sequences.¹

Algorithm 1 SWORD: Spectral Wasserstein Online Regime Detection

Input: Graph stream G_1, G_2, \dots ; threshold θ ; test window w ; reference window w_{ref} ; cooldown c ; moments k ; distance mode $\text{mode} \in \{D_t^{\text{pw}}, D_t^{\text{cen}}, D_t^{\Gamma}\}$ (Theorem 4.2); window weighting (uniform or exponential)

Output: Detected change points (output incrementally)

Initialize $\tau_{\text{prev}} \leftarrow -\infty$

for $t = 1, 2, \dots$ (**as each** G_t **arrives**) **do**

$\mu_t \leftarrow k$ Chebyshev moments of G_t via KPM

if $t \geq w + w_{\text{ref}}$ **then**

$D_t \leftarrow$ two-window statistic (per chosen mode) over $\mu_{t-w-w_{\text{ref}}+1:t}$

if $D_t \geq \theta$ **and** $t - \tau_{\text{prev}} \geq c$ **then**

output t as change point

$\tau_{\text{prev}} \leftarrow t$

end if

end if

end for

4.5 Detection Algorithm

Algorithm 1 summarizes the procedure. The first $w + w_{\text{ref}}$ steps serve as a burn-in. As the test window slides over a true change point the statistic D_t ramps up and back down, so the cooldown c suppresses repeat alarms from a single change. The threshold θ is set via grid search or as a percentile of the burn-in D_t values. KPM dominates the per-step cost at $O(KRm)$ (the two-window comparison adds a negligible $O(w w_{\text{ref}} k)$), giving total $O(TKRm)$ across T snapshots—linear in edges.

5 Experiments

Baselines. Eight baselines from three families. *Spectral/graph*: SCPD (Huang et al., 2023), LADdos (Huang et al., 2021), LAD (Huang et al., 2020). *Feature-based* (on an 8-dim feature vector): CUSUM (Page, 1954), EWMA (Roberts, 1959), BOCPD (Adams and MacKay, 2007), MMD (Gretton et al., 2012). *Training-based*: TIRE (De Ryck et al., 2021), an offline autoencoder with a time-invariance loss; trains unsupervised on the full test sequence and is therefore retrospective.

Datasets. Table 1 summarizes the benchmarks: synthetic with large effect sizes (single CP at $t=50$; two for Multi-CP) and real-world spanning three scales from MIT Reality (63 nodes, daily) to Enron (86,664 nodes, weekly).

¹Stationary residuals hold only approximately on real data (linear-trend slopes are detectable, $p < 10^{-6}$). Operationally, drift stays below threshold: under each tuned threshold the spurious detections are 0 on Enron and AskUbuntu and 2/6 on MIT, despite Enron’s second-half mean score being $\sim 8\times$ the first-half mean.

Table 1: Benchmark datasets. CPs = ground-truth change points.

Dataset	Type	Nodes	Graphs	CPs
ER	Random	100	100	1
SBM	Community	100	100	1
BA	Scale-free	100	100	1
WS	Small-world	100	100	1
Multi-CP	Mixed	100	150	2
MIT Reality	Proximity	63	270	6
AskUbuntu	Q&A	~4,663	76	11
Enron	Email	86,664	200	5

Evaluation. We use *one-sided* matching: a detection $\hat{\tau}$ is a true positive iff $\hat{\tau} \in [\tau^*, \tau^* + \delta]$ for some unmatched true change point τ^* ; detections outside every such window are false positives. Following [Truong et al. \(2020\)](#), each tolerance satisfies $\delta < \text{min-gap}$ and scales with temporal resolution: $\delta=5$ (synthetic and MIT), $\delta=2$ (AskUbuntu), $\delta=4$ (Enron).

Hyperparameter search. Each method gets 2,700–5,000 grid configurations: SWORD searches seven parameters ($\theta, w, w_{\text{ref}}, k, c$, distance mode, weighting) versus 3–4 for baselines (Section B), so at matched budget baselines get denser per-axis coverage. Stochastic methods (SWORD, SCPD) cross-validate over 5 moment seeds; synthetic data over 10 graph seeds. KPM is fixed at $K=50$, $R=30$.

5.1 Results

Detection accuracy. Figure 1 shows the qualitative gap: SWORD’s two-window L_1 statistic pulses sharply at each true change point, while baselines drift, lock onto the burn-in, or pulse much more weakly. Table 2 quantifies it. Among online methods, SWORD achieves the highest precision (0.91, only 2 FPs vs. 19–31 for CUSUM/LAD/EWMA) and the highest per-dataset F_1 on every benchmark (mean 0.79). F_1 is stable across Hutchinson seeds (± 0.00 –0.03); SCPD’s seed variance grows where its score saturates (Enron, below).

SCPD controlled comparison. LADdos—which differs from SCPD only in per-window clamping—scores within 0.04 F_1 of SCPD on every dataset, so the SCPD to SWORD gap is architectural, not an implementation artifact.

We walk one design axis at a time from SCPD’s scoring pipeline to SWORD’s, holding the input fixed (Jackson-filtered KPM moments with SCPD’s per-dataset best windows and moment count k , mean-pairwise aggregation throughout). The cascade: **S0** is SCPD’s untuned scoring on this fixed input (SVD + cosine + first-difference)—not the per-dataset tuned SCPD row of Table 2. **S1** replaces SVD with a window mean. **S2** drops the first-difference. **S3** swaps the single-point score for a two-window comparison; cosine is unchanged through here. **S3**¹/₂ switches cosine to L_1 on L_2 -normalized inputs, isolating the metric from scale. **S4** removes L_2 normalization. **S5** removes Jackson filtering, recovering full SWORD. SWORD-only knobs (notably asymmetric windowing) sit outside this controlled cascade and are flagged separately below.

The dominant in-scaffold mechanism is dataset-dependent:

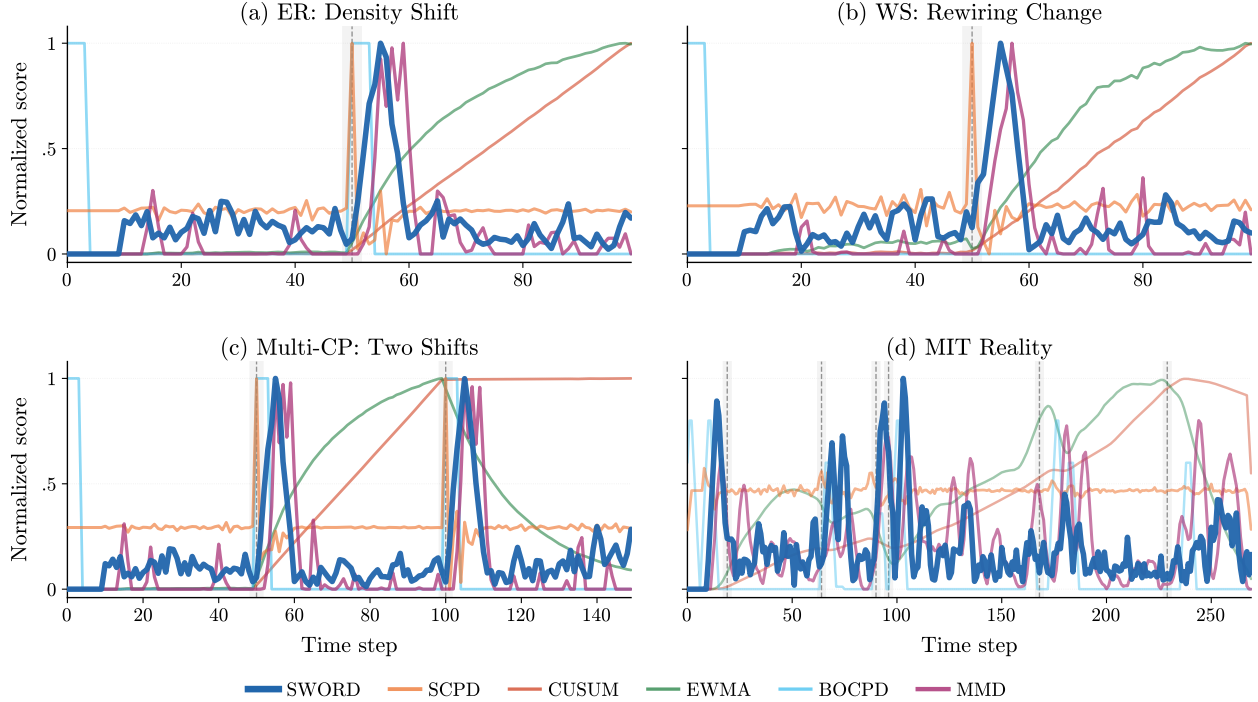


Figure 1: Detection signals on three synthetic benchmarks (a–c) and MIT Reality (d). Vertical dashed lines mark true change points; scores normalized to $[0, 1]$ per series. SWORD (bold blue) produces pulses at each change point; CUSUM/EWMA drift, BOCPD locks onto the burn-in, and SCPD’s pulses are visibly smaller for MIT despite sharing SWORD’s KPM moments.

- **MIT** (sudden events, 63-node). The two-window mean (S3) closes most of the gap ($+0.23 F_1$); reducing k from 30 to 8 adds $+0.08$, leaving a $+0.03$ residual to SWORD’s per-dataset best.
- **Enron** (slow drift, 86K-node). With the two-window structure fixed, swapping cosine for L_1 ($S3 \rightarrow S3\frac{1}{2}$, both on L_2 -normalized inputs) closes the gap ($+0.50 F_1$). On 86K-node graphs consecutive moment vectors differ by tiny amounts; the cosine of two adjacent unit vectors saturates near 1 while L_1 preserves the displacement. The score size confirms it: SCPD’s peak on Enron is $\sim 2 \times 10^{-5}$, two orders below the lowest threshold in our grid (0.005), so no SCPD configuration detects. This is the W_1/L_1 connection of Theorem 4.1, sharp on the largest network.
- **AskUbuntu** (periodic, 4.6K-node). The in-scaffold cascade plateaus at $F_1 = 0.53$. The residual to SWORD’s 1.00 closes only with asymmetric windowing ($w=2, w_{\text{ref}}=5$), a SWORD-only knob outside SCPD’s parameter space. This residual is therefore *uncontrolled* relative to SCPD—a hyperparameter SCPD has no equivalent of, not an architectural attribution.

A separate bin-width sweep (Figure 3) shows F_1 is flat past 32 bins on every dataset and remains below SWORD’s per-dataset F_1 at every bin count tested, including the $n_{\text{bins}}=\infty$ point that drops the histogram step entirely. Histogram discretization is the most visible architectural difference between SCPD’s published pipeline and SWORD’s, but on these benchmarks it does not drive the F_1 gap.

Generalization. The “Fixed-cfg (in-sample)” column picks a single configuration maximizing mean F_1 on those same three datasets—an in-sample fit, not a deployable operating point. SWORD

Table 2: Real-world detection quality under one-sided matching. F_1 is cross-validated over 5 moment seeds for stochastic methods (SWORD, SCPD), single evaluation otherwise; \pm is std across seeds. **Fixed-cfg** is the best single config *selected in-sample* across the three datasets—an in-sample fit, not a deployment number. [†]TIRE-legacy uses the original benchmark PyTorch environment; TIRE-current uses PyTorch 2.11, which shifts `nn.Linear` default initialization and lowers Enron F_1 from 0.86 to 0.58 (Section I). Computational cost is reported separately in Table 3.

Method	Per-Dataset F_1 (tuned)			Mean F_1	Fixed-cfg	Quality	
	MIT	AskU	Enron			Prec.	Rec.
CUSUM	0.46	0.67	0.38	0.50	0.39	0.35	0.86
EWMA	0.46	0.73	0.46	0.55	0.39	0.46	0.77
BOCPD	0.50	0.70	0.40	0.53	0.38	0.50	0.58
MMD	0.60	0.96	0.50	0.69	0.46	0.72	0.67
SCPD	0.53 \pm .07	0.29 \pm .04	0.00	0.27	0.20	0.38	0.22
LADdos	0.49 \pm .05	0.29 \pm .04	0.00	0.27	—	0.36	0.21
LAD	0.67	0.91	0.33	0.64	0.47	0.59	0.86
TIRE-legacy [†]	0.75	0.76	0.86	0.79	—	0.72	0.82
TIRE-current [†]	—	—	0.58	—	—	—	—
SWORD	0.69\pm.03	1.00	0.67	0.79	0.50	0.91	0.72

Table 3: Real-world computational cost. **Runtime**: end-to-end seconds from raw graphs. **Memory**: peak resident MB per dataset.

Method	Runtime (s)			Memory (MB)		
	MIT	AskU	Enron	MIT	AskU	Enron
CUSUM	0.4	7.9	527	0.1	4.4	31.3
EWMA	0.4	7.6	488	0.1	4.4	31.3
BOCPD	0.4	7.9	404	0.4	4.4	31.3
MMD	0.4	7.3	426	0.1	4.4	31.3
SCPD	13.3	107	390	0.2	4.7	13.9
LADdos	13.3	107	390	0.2	4.7	13.9
LAD	0.5	5.6	328	0.3	5.0	30.8
SWORD	13.0	117	385	0.2	4.8	13.9

reaches 0.50, only 0.04 above MMD; every method loses 0.07–0.29 F_1 versus per-dataset tuning, reflecting benchmark diversity (daily 63-node proximity vs. weekly 86K-node email). The per-dataset numbers in Table 2 similarly lack held-out validation and characterize the achievable, not the deployable, operating point. A few-shot calibration experiment (Section H) recovers the gap on MIT and AskUbuntu but *hurts* Enron, so sparse-label calibration is not a general fix.

Scalability. Runtime ordering depends on graph size. On Enron (86K nodes) KPM methods win—SWORD 385s, SCPD 390s vs. 404–527s for feature methods, with the least memory (13.9 vs. 31.3 MB)—because KPM’s inner loop is sparse matvecs scaling in $|E|$. On AskUbuntu (\sim 4.6K

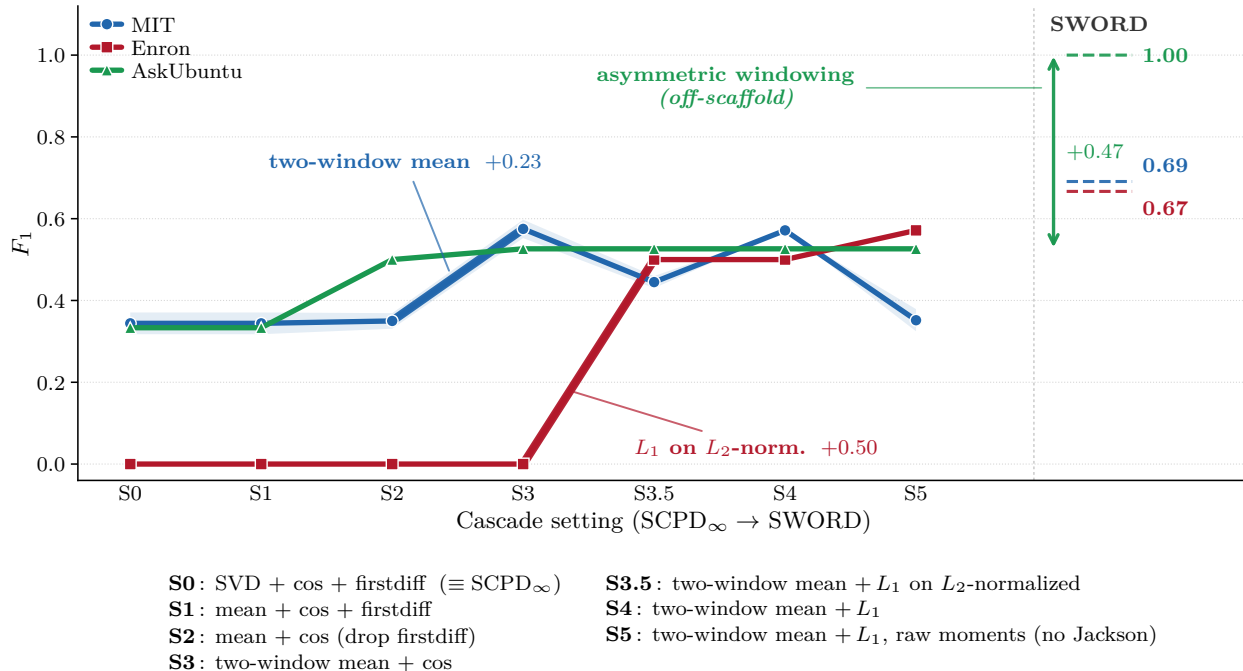


Figure 2: **Cascading architectural ablation (SCPD $_{\infty}$ \rightarrow SWORD)**. Held fixed: Jackson-filtered KPM moments at $n_{\text{bins}}=\infty$ and SCPD’s per-dataset best n_{moments} , windows, cooldown. Each cascade step changes one axis (legend below the panel). Connected slopegraph plots mean F_1 over 5 stochastic seeds, with ± 1 std as the shaded band; per-dataset SWORD references appear as dashed ticks on the right margin. For MIT and Enron the gap is closed by a single in-scaffold axis (annotated): the two-window mean (+0.23) and the L_1 metric on L_2 -normalized inputs (+0.50), respectively. For AskUbuntu the scaffold plateaus at 0.53 and the +0.47 residual to SWORD is closed by asymmetric windowing (right-margin arrow)—a hyperparameter outside SCPD’s parameter space.

nodes) the order flips: LAD (6s) and feature methods (7–8s) are fastest while KPM (107–117s) lags, as $KR = 1,500$ matvecs per graph dominate at this size.

False-alarm and delay tradeoff. Table 4 reports ARL_0 (steps to first false alarm under H_0) and ADD (delay after a true change), measured on ER graphs ($n=50$, 100 seeds) at matched false-alarm rate; Figure 4 plots the full ADD-vs.- $\log_{10} ARL_0$ curves at $\Delta p \in \{0.05, 0.10\}$. CUSUM/EWMA achieve the lowest ADD on the large shift. On the small shift SWORD is the only method maintaining 100% detection across all operating points (LAD 0%, SCPD 69%, MMD 92%), at a cost of about 3 steps of delay.

Synthetic results. At easy effect sizes (Table 5; 10 seeds, cross-validated), SWORD, SCPD, LADdos, and BOCPD all reach 1.00. Saturation hides differences, so we probe whether the per-dataset mechanisms transfer to harder contrasts. SWORD’s L_1 advantage holds on small ER density shifts where cosine saturates. On SBM community-merge shifts (Table 6), SWORD and SCPD tie within 0.05 F_1 and feature-based baselines lead at high contrast: the block-merge causes a large eigenvector reconfiguration cosine registers as readily as L_1 , and feature statistics like mean degree

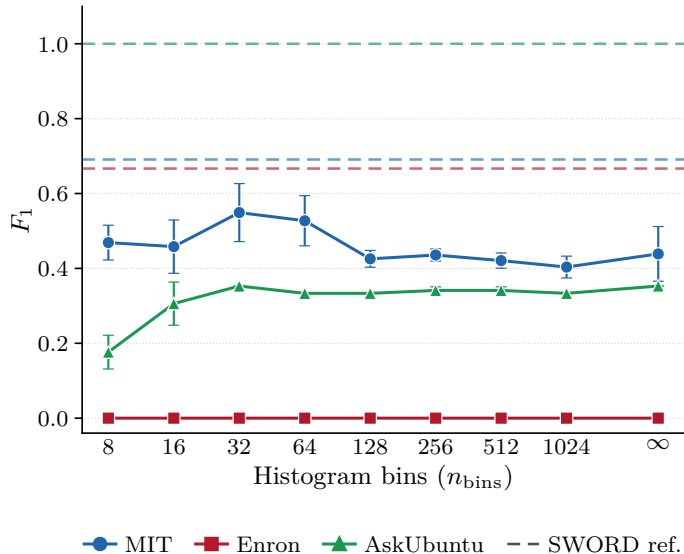


Figure 3: **Bin-width sweep on SCPD.** Holding the SCPD pipeline at its per-dataset best, the histogram bin count is varied from 8 to 1024, plus an “ ∞ ” point that drops the histogram step entirely. Mean F_1 over 5 stochastic seeds; error bars are ± 1 std. SWORD’s per-dataset F_1 is shown as a dashed reference.

Table 4: Method properties beyond F_1 . **ARL₀/ADD**: at matched false-alarm rate on ER ($n=50$, $p=0.1 \rightarrow 0.2$, 100 seeds). **FP**: total false positives across the three real-world datasets. **Delay**: mean detection delay (steps after true CP). **Cost**: per-graph complexity (d =feature dimension).

Method	ARL ₀	ADD	FP	Delay	Cost
CUSUM	211	0.7	31	2.7	$O(d)$
EWMA	240	0.1	20	3.7	$O(d)$
BOCPD	500	0.0	11	3.4	$O(Td)$
MMD	473	5.5	4	3.6	$O(w^2d)$
SCPD	418	0.0	4	6.0	$O(KRm)$
LADdos	418	0.0	5	5.9	$O(KRm)$
LAD	236	50.0	19	1.6	$O(n^3)$
SWORD	220	2.4	2	3.1	$O(KRm)$

shift sharply enough for BOCPD and MMD to win. The Enron cosine-saturation story therefore does not transfer to abrupt structural change.

6 Limitations

1. **Configuration sensitivity.** Every method loses F_1 moving from per-dataset-tuned to a single fixed config (SWORD $0.79 \rightarrow 0.50$; MMD $0.69 \rightarrow 0.46$). The gap reflects structural variation in optimal k , window length, distance mode, and threshold (Section B), not threshold alone. A few-shot protocol (Section H) lifts MIT and AskUbuntu but hurts Enron, where a single label

Table 5: Synthetic F_1 (mean \pm std, 10 seeds, cross-validated, one-sided $\delta=5$). SWORD and SCPD achieve perfect detection on all five types.

Method	ER	SBM	BA	WS	Multi
CUSUM	.40	.45 \pm .05	.40	.43 \pm .05	.50
EWMA	.42 \pm .04	.44 \pm .08	.40	.42 \pm .04	.50
BOCPD	1.00	1.00	1.00	.50	1.00
MMD	.97 \pm .10	1.00	1.00	1.00	.98 \pm .06
SCPD	1.00	1.00	1.00	1.00	1.00
LADdos	1.00	1.00	1.00	1.00	1.00
LAD	.71 \pm .21	.20 \pm .16	.43 \pm .45	.56 \pm .36	.70 \pm .22
SWORD	1.00	1.00	1.00	1.00	1.00

Table 6: Hard SBM stress test ($n=60$, $p_{\text{in}}=0.30$, 3-block \rightarrow 2-block; SBM-family-tuned, 20 seeds). Three representative rows from Table 9.

p_{out}	SWORD	SCPD	BOCPD	MMD	LAD
0.02	0.45	0.50	0.90	0.93	0.13
0.05	0.68	0.68	0.92	0.87	0.08
0.10	0.44	0.58	0.75	0.45	0.10

overfits; mean F_1 stays near 0.50 for $N \leq 3$. Label-free e-process sequential testing (Shin et al., 2022) is a more promising direction.

- Loose approximation constant.** As noted under Theorem 4.1, C/k exceeds $W_1^{\text{max}}=2$ for practical $k = 2-7$, so the theorem is design rationale rather than an operational guarantee. A distribution-dependent bound paired with a Hutchinson variance–bias decomposition would tighten the small- k analysis (Section J).
- Cospectral graphs.** Non-isomorphic graphs can share spectra (van Dam and Haemers, 2003), making such changes invisible to any spectrum-only detector, SWORD included. Augmenting moments with complementary invariants (e.g., triangle counts) could reduce this blind spot.

7 Conclusion

Diagnostic: within SCPD’s scoring scaffold, the SCPD–SWORD gap is driven by comparison structure and the L_1 metric, not histogram discretization—structure on MIT, L_1 on Enron. Whether this attribution generalizes beyond the SCPD-derived scaffold is open.

Detector: among online methods SWORD attains the highest precision and reaches mean $F_1 = 0.79$, matching TIRE’s published value; TIRE’s Enron drops to 0.58 in our PyTorch 2.11 reimplementation, and forcing TIRE online preserves parity with TIRE-current (Section I). SWORD differs from TIRE on three scale-robust axes: no training step, an interpretable spectral statistic in place of a learned latent dimension, and linear-in-edges cost—decisive on Enron, less so at AskUbuntu scale where TIRE stays competitive.

Threshold-free detection without labels is the main open challenge. Integrating e-process sequential testing (Shin et al., 2022) with SWORD’s statistics is a natural next step; a second is extending beyond the normalized Laplacian to weighted, directed, or signed graphs via analogous operators.

Reproducibility Statement

All experiments run on a single workstation (Intel i9, 64 GB RAM, RTX 4090) with deterministic seeds. Each method receives 2,700–5,000 grid-search configurations, selected by cross-validated mean F_1 (10 graph seeds for synthetic, 5 moment-estimation seeds for stochastic real-world methods). KPM is fixed at $K = 50$ moments, $R = 30$ Hutchinson probes. Datasets, evaluation protocol, and selected hyperparameters are in Appendices A–B; distance-mode and window-configuration ablations are in Appendices E–F.

References

- R. P. Adams and D. J. C. MacKay. Bayesian online changepoint detection. *arXiv preprint arXiv:0710.3742*, 2007.
- V. Braverman, A. Krishnan, and C. Musco. Sublinear time spectral density estimation. In *Proceedings of the 54th Annual ACM SIGACT Symposium on Theory of Computing (STOC)*, pages 1144–1157, 2022. doi: 10.1145/3519935.3520009. arXiv:2104.03461.
- T. De Ryck, M. De Vos, and A. Bertrand. Change point detection in time series data using autoencoders with a time-invariant representation. In *IEEE International Conference on Acoustics, Speech and Signal Processing (ICASSP)*, pages 3720–3724, 2021.
- K. Dong, A. R. Benson, and D. Bindel. Network density of states. In *Proceedings of the 25th ACM SIGKDD International Conference on Knowledge Discovery and Data Mining*, pages 1152–1161, 2019.
- F. Enikeeva and O. Klopp. Change-point detection in dynamic networks with missing links. *Operations Research*, 73(5):2417–2429, 2025. doi: 10.1287/opre.2021.0413.
- A. Gretton, K. M. Borgwardt, M. J. Rasch, B. Schölkopf, A. Smola, et al. A kernel two-sample test. *Journal of Machine Learning Research*, 13:723–773, 2012.
- J. Gu, B. Hua, and S. Liu. Spectral distances on graphs. *Discrete Applied Mathematics*, 190–191: 56–74, 2015.
- S. S. Ho, T. T. Kairamkonda, and I. Ali. Detecting and explaining structural changes in an evolving graph using a martingale. *Pattern Recognition*, 169:111855, 2025. doi: 10.1016/j.patcog.2025.111855.
- S. Huang, Y. Hitti, G. Rabusseau, and R. Rabbany. Laplacian change point detection for dynamic graphs. In *Proceedings of the 26th ACM SIGKDD International Conference on Knowledge Discovery and Data Mining*, pages 349–358, 2020.
- S. Huang, G. Rabusseau, and R. Rabbany. Scalable change point detection for dynamic graphs. In *ODD Workshop at KDD*, 2021.
- S. Huang, J. Danovitch, G. Rabusseau, and R. Rabbany. Fast and attributed change detection on dynamic graphs with density of states. In *Advances in Knowledge Discovery and Data Mining (PAKDD)*, pages 15–26, 2023.
- M. F. Hutchinson. A stochastic estimator of the trace of the influence matrix for Laplacian smoothing splines. *Communications in Statistics—Simulation and Computation*, 19(2):433–450, 1990.

- T. Ideker and N. J. Krogan. Differential network biology. *Molecular Systems Biology*, 8(1):565, 2012.
- Y. Kei, J. Li, Y. Chen, and O. H. M. Padilla. Change point detection on a separable model for dynamic networks. *Transactions on Machine Learning Research*, 2025. arXiv:2303.17642.
- D. Koutra, N. Shah, J. T. Vogelstein, B. Gallagher, and C. Faloutsos. DeltaCon: Principled massive-graph similarity function with attribution. *ACM Transactions on Knowledge Discovery from Data*, 10(3):1–43, 2016.
- L. Lin, Y. Saad, and C. Yang. Approximating spectral densities of large matrices. *SIAM Review*, 58(1):34–65, 2016.
- G. Lorden. Procedures for reacting to a change in distribution. *The Annals of Mathematical Statistics*, 42(6):1897–1908, 1971.
- Y. Mei, D. Xu, Y. Wang, X. Wei, X. Tang, and Z. Han. A survey of change point detection in dynamic graphs. *IEEE Transactions on Knowledge and Data Engineering*, 2025. doi: 10.1109/TKDE.2024.3523857.
- C. Musco, C. Musco, L. Rosenblatt, and A. V. Singh. Sharper bounds for Chebyshev moment matching with applications. In *Proceedings of the 38th Annual Conference on Learning Theory (COLT)*, 2025. arXiv:2408.12385.
- R. Musco and C. Musco. Improved spectral density estimation via explicit and implicit deflation. *Proceedings of the ACM-SIAM Symposium on Discrete Algorithms (SODA)*, 2025.
- E. S. Page. Continuous inspection schemes. *Biometrika*, 41(1/2):100–115, 1954.
- L. Peel and A. Clauset. Detecting change points in the large-scale structure of evolving networks. In *Proceedings of the 29th AAAI Conference on Artificial Intelligence*, pages 2914–2920, 2015.
- S. W. Roberts. Control chart tests based on geometric moving averages. *Technometrics*, 1(3):239–250, 1959.
- J. Shin, A. Ramdas, and A. Rinaldo. E-detectors: A nonparametric framework for sequential change detection. *arXiv preprint arXiv:2203.03532*, 2022.
- C. Truong, L. Oudre, and N. Vayatis. Selective review of offline change point detection methods. *Signal Processing*, 167:107299, 2020.
- A. Tsitsulin, D. Mottin, P. Karras, A. Bronstein, and E. Müller. NetLSD: Hearing the shape of a graph. In *Proceedings of the 24th ACM SIGKDD International Conference on Knowledge Discovery and Data Mining*, pages 2347–2356, 2018.
- E. R. van Dam and W. H. Haemers. Which graphs are determined by their spectrum? *Linear Algebra and its Applications*, 373:241–272, 2003.
- A. Weiße, G. Wellein, A. Alvermann, and H. Fehske. The kernel polynomial method. *Reviews of Modern Physics*, 78(1):275–306, 2006.

A Experimental Setup

Synthetic data. We generate 100-graph sequences ($n = 100$) with one change point at $t = 50$, or two at $t = 50, 100$ for Multi-CP (150 graphs). Each type tests a distinct mechanism: ER shifts edge probability $p=0.1 \rightarrow 0.3$ (density); SBM merges three communities into two at fixed $p_{\text{in}}=0.3, p_{\text{out}}=0.02$ (community reorganization); BA shifts preferential-attachment $m=2 \rightarrow 5$ (degree distribution); WS shifts rewiring $p=0.1 \rightarrow 0.5$ (small-world disruption).

MIT Reality: 270 daily Bluetooth proximity graphs (63 nodes) with academic calendar events (Columbus Day, Thanksgiving, Christmas, New Year, Spring Break, semester end). **AskUbuntu:** 76 monthly Q&A interaction graphs ($\sim 4,663$ nodes) with Ubuntu releases (10.10–15.10) as ground truth. **Enron:** 200 weekly email graphs (86,664 nodes) with Skilling becoming CEO, his resignation, loss announcements, and the SEC probe / Dynegy merger collapse (the last two, one week apart, merged into a single change point at week 160).

Baselines. CUSUM operates on the 8-dim feature vector via Page’s two-sided tabular form, $S_t^\pm = \max(0, S_{t-1}^\pm \pm z_t - \kappa)$ with z_t standardized from burn-in only; a detection fires when $\max_d \max(S_t^{+(d)}, S_t^{-(d)}) \geq \theta$. Other baselines follow standard implementations; exact hyperparameter ranges are in the accompanying code release.

B Hyperparameters

Table 7 lists SWORD’s best parameters per dataset from the 5,000-configuration grid search. Baseline parameter details are in the accompanying code release.

Table 7: SWORD’s best hyperparameters per dataset from 5,000 grid search configurations. Synthetic: cross-validated (best mean F_1 over 10 graph seeds). Real-world: cross-validated over 5 moment-estimation seeds. Parameters: θ =detection threshold (p =percentile-based), w/w_{ref} =test/reference window, k =Chebyshev moments, c =cooldown, Mode=distance aggregation (see Section E).

Dataset	θ	w	w_{ref}	k	c	Mode	F_1
ER	0.02	3	3	2	5	weighted- Γ	1.00
SBM	0.02	4	4	2	7	weighted- Γ	1.00
BA	0.05	2	2	2	15	weighted- Γ	1.00
WS	0.02	7	7	3	15	weighted- Γ	1.00
Multi-CP	0.02	3	3	2	5	weighted- Γ	1.00
MIT Reality	$p=0.84$	7	7	2	10	mean-pw (D_t^{pw})	0.69
AskUbuntu	$p=0.20$	2	5	2	6	mean-pw (D_t^{pw})	1.00
Enron	0.005	2	2	4	7	weighted- Γ	0.67

C Hard Synthetic Benchmarks

The main-text synthetic benchmarks saturate at $F_1 \approx 1.0$. We re-test at small effect sizes on two change types (density shifts on ER, community-merge on SBM) to probe whether the cascading attribution generalizes.

Hard ER (density shifts, fixed-cfg params). We sweep $p_2 \in [0.15, 0.40]$ on ER graphs ($n = 50$, $T = 100$, 20 seeds, $\delta = 5$), with all methods at their fixed-cfg (in-sample) parameters.

Table 8: F_1 on hard synthetic ER graphs ($n=50$, $p_1=0.10$, varying p_2 ; mean over 20 seeds) with fixed-cfg (in-sample) parameters. SWORD dominates across all effect sizes. [†]LADdos uses SCPD’s fixed-cfg parameters (algorithmically equivalent for global CPD).

p_2	SWORD	SCPD	LADdos [†]	LAD	CUSUM	EWMA	BOCPD	MMD
0.15	0.91	0.64	0.64	0.05	0.11	0.26	0.12	0.13
0.18	1.00	0.67	0.67	0.03	0.11	0.27	0.12	0.14
0.20	1.00	0.67	0.67	0.00	0.11	0.27	0.11	0.13
0.22	1.00	0.69	0.69	0.00	0.11	0.27	0.11	0.13
0.25	1.00	0.69	0.69	0.00	0.11	0.27	0.11	0.13
0.30	1.00	0.69	0.69	0.00	0.11	0.27	0.11	0.13
0.40	1.00	0.69	0.69	0.00	0.11	0.27	0.11	0.13

SWORD leads at every effect size with its fixed-cfg parameters ($\theta=0.005$, $w=2$, $k=4$, weighted- Γ), reaching $F_1 = 0.91$ at $\Delta p = 0.05$ and $F_1 = 1.00$ for $\Delta p \geq 0.08$. This in-sample optimum coincides with Enron’s per-dataset best because the same low threshold, calibrated to Enron’s subtle spectral shifts, transfers to small density shifts. SCPD plateaus at $F_1 \approx 0.69$, consistent with the cosine-saturation mechanism in Section 5.1.

Hard SBM (community contrasts, SBM-family-tuned params). A 3-block SBM (pre-change) merges to 2 blocks (post-change) at fixed $p_{\text{in}} = 0.30$, with $p_{\text{out}} \in [0.02, 0.25]$ swept. Smaller p_{out} gives a larger structural-merge signal; $p_{\text{out}} \rightarrow p_{\text{in}}$ approaches ER. Fixed-cfg parameters miscalibrate at this scale, so we report each method’s SBM-family best (grid-searched on the main-text SBM benchmark, evaluated on the hard variants).

Table 9: F_1 on hard SBM ($n=60$, $p_{\text{in}}=0.30$, 3-block \rightarrow 2-block at $t=50$; mean over 20 seeds) under each method’s SBM-family best parameters (see Section B). SCPD/SWORD/BOCPD/MMD all detect high-contrast merges; SCPD and SWORD are within 0.05 F_1 of each other across all contrasts.

p_{out}	SWORD	SCPD	BOCPD	MMD	LAD	CUSUM	EWMA
0.02	0.45	0.50	0.90	0.93	0.13	0.07	0.18
0.05	0.68	0.68	0.92	0.87	0.08	0.00	0.00
0.08	0.58	0.56	1.00	0.72	0.15	0.00	0.02
0.10	0.44	0.58	0.75	0.45	0.10	0.00	0.00
0.15	0.00	0.10	0.05	0.23	0.10	0.00	0.00
0.20	0.00	0.00	0.00	0.18	0.05	0.00	0.00
0.25	0.00	0.00	0.00	0.05	0.07	0.00	0.00

SWORD and SCPD track each other within 0.05 F_1 at every contrast: swapping cosine for L_1 on the same KPM moments produces nothing like the +0.50 Enron gap, because the block-merge causes a sharp eigenvector reconfiguration cosine registers as readily as L_1 . BOCPD and MMD lead at high contrast: the block-merge produces a sharp discontinuity in feature statistics (mean degree,

edge count, density) both methods are calibrated to flag. The cascading attribution therefore is regime-specific— L_1 dominates Enron’s slow drift but not SBM’s abrupt structural change.

D ARL/ADD Trade-off Curves

Figure 4 sweeps detection thresholds on ER graphs ($n=50$, 100 seeds, $T=500$ null / $T=100$ change) to map the full ARL_0 -detection trade-off at two effect sizes. Detection rate (top row) and ADD (bottom row, where detection rate ≥ 0.3) are plotted against $\log_{10}(ARL_0)$. On the large shift most methods maintain high detection rate across a wide ARL_0 range and CUSUM/EWMA achieve the lowest ADD. On the small shift, LAD drops to 0%, SCPD to 69%, MMD to 92%, while SWORD holds 100% throughout.

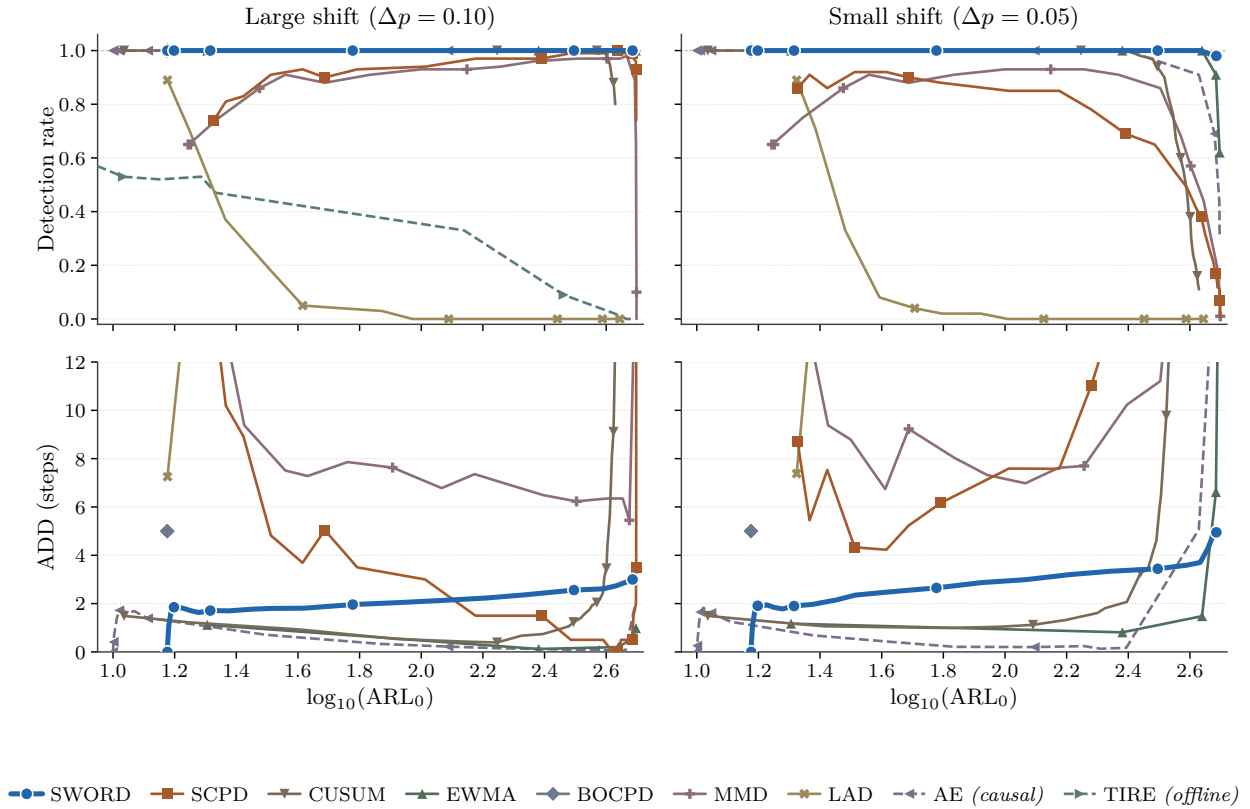


Figure 4: False-alarm vs. detection trade-off. Top row: detection rate (power) vs. $\log_{10}(ARL_0)$. Bottom row: ADD vs. $\log_{10}(ARL_0)$ (where detection rate ≥ 0.3). Left: large shift ($\Delta p = 0.10$). Right: small shift ($\Delta p = 0.05$). SWORD (blue) maintains 100% detection across all swept operating points in both conditions.

E Distance Metric Ablation

SWORD’s two-window statistic offers three distance modes (prose names in main text, code names in parentheses): **mean-pairwise** (`mean_pairwise`, D_t^{pw} , Equation (6))—mean over pairwise L_1 distances; **centroid- L_1** (`mean_distance`, D_t^{cen} , Equation (7))— L_1 between window means;

weighted- Γ (`weighted_gamma`, D_t^Γ , Equation (8))—the weighted discrepancy Γ from Theorem 4.1 on window means.

Table 10: Best F_1 for each of SWORD’s three distance modes with per-dataset tuned parameters (MIT $\delta=5$, AskUbuntu $\delta=2$, Enron $\delta=4$; all one-sided). Mean-pairwise is best or tied-best on all three datasets; the centroid- L_1 and weighted- Γ modes are retained in the grid search as alternatives that match the same F_1 on Enron.

Distance Mode	MIT	AskUbuntu	Enron
mean-pairwise (D_t^{pw})	0.69	1.00	0.67
centroid- L_1 (D_t^{cen})	0.67	0.86	0.67
weighted- Γ (D_t^Γ)	—	0.77	0.67

Mean-pairwise dominates on MIT and AskUbuntu, and all three modes tie on Enron at $F_1 = 0.67$. Weighted- Γ does not appear in the MIT top-50 (“—”), indicating pairwise and centroid formulations are more effective on small, dense graphs.

F Window Configuration Ablation

Table 11 reports the best F_1 from the grid search top-50 configs for each of SWORD’s three window configurations (Section 4.4).

Table 11: Best F_1 for each of SWORD’s window configurations (per-dataset tuned). Asymmetric windows achieve perfect F_1 on AskUbuntu; symmetric suffices on MIT and Enron.

Window Config	MIT	AskUbuntu	Enron
Symmetric	0.69	0.78	0.67
Asymmetric	0.67	1.00	0.67
Exp-weighted	0.68	0.83	0.67

The asymmetric configuration ($w=2$, $w_{\text{ref}}=5$) is decisive on AskUbuntu, where 11 change points are 6 months apart: a short test window responds within the tight $\delta=2$ tolerance while a long reference stays stable. On MIT and Enron, sparser CPs and wider tolerances let symmetric windows suffice. All three configurations tie at $F_1 = 0.67$ on Enron, where graph size (86K nodes) dominates over window design.

G Training-Based and Additional Spectral Baselines

LADdos. LADdos (Huang et al., 2021) sits between LAD (Huang et al., 2020) and SCPD (Huang et al., 2023), replacing LAD’s exact eigenvalue signatures with KPM-approximated DOS histograms while keeping the same two-window SVD + cosine detection. The only algorithmic difference from SCPD is the order of two operations: LADdos clamps the first-difference Z^* to non-negative per window before taking the max, whereas SCPD takes the max first then differences. With $\sim 3,000$

grid configurations LADdos lands within 0.04 F_1 of SCPD on every dataset, confirming functional equivalence for global CPD.

TIRE. TIRE (De Ryck et al., 2021) is an offline, unsupervised autoencoder CPD method that trains on the full sequence with a time-invariance penalty. We reimplement the full algorithm (paired TD/FD autoencoders with $K+1$ parallel windows, Jackson-filtered DOS, matched-filter post-processing); the grid covers all key hyperparameters ($N, K, h, s, \lambda, \text{domain}$), 16,200 configurations per dataset. TIRE reaches mean $F_1 = 0.79$, identical to SWORD, but retrospectively.

H Few-Shot Calibration

We test whether a small number of labeled change points can close the gap between fixed-cfg ($F_1 = 0.50$) and per-dataset best ($F_1 = 0.79$).

Protocol. The configuration pool has four candidates: the fixed-cfg SWORD configuration plus the per-dataset best on each of the three real-world datasets. For target dataset T and N labeled CPs, we sample subsets S of size N from T ’s ground truth, score every pool config by $F_1(S)$, pick the best, and report test F_1 on $T_{\text{true}} \setminus S$. $N=0$ uses fixed-cfg; $N=\text{“all”}$ is the oracle. Five stochastic seeds.

Result. Figure 5 plots test F_1 vs. N . At $N=1$ the protocol lifts MIT ($0.27 \rightarrow 0.46$) and AskUbuntu ($0.57 \rightarrow 0.71$) but *hurts* Enron ($0.67 \rightarrow 0.29$), whose fixed-cfg is already near-optimal: with a single labeled CP, calibration F_1 is dominated by detection sparsity (precision is $1/(\# \text{ detections})$), so a config detecting only the labeled CP beats fixed-cfg at calibration even while missing most CPs at test. Mean F_1 across datasets stays near 0.50 for $N \leq 3$. The oracle recovers per-dataset best in every case, so the gap is closeable in principle but not by sparse labels.

I Online TIRE Robustness

We test whether TIRE’s $F_1 = 0.79$ depends on offline access to the test sequence by retraining on a bounded prefix $[0, T_{\text{warm}}]$, freezing the model, and scoring the full sequence with frozen weights. All TIRE hyperparameters are at per-dataset best; only T_{warm} varies. Five SGD seeds; threshold re-tuned per cell.

Result. At $T_{\text{warm}} = 0.25T$, TIRE on Enron achieves $F_1 = 0.71$, exceeding offline TIRE (0.58 in our environment); AskUbuntu shows the same direction; MIT is roughly flat. Training on the full sequence forces the autoencoder to reconstruct both pre- and post-CP regimes, diluting the time-invariant latent space’s sensitivity to the shift. Offline access is therefore not the source of TIRE’s detection performance; on Enron and AskUbuntu it works against it.

Note on absolute scale. F_1 values here are lower than the TIRE-legacy row of Table 2 because of PyTorch version drift (the legacy row used TIRE’s original environment; this appendix uses PyTorch 2.11 with current `nn.Linear` initialization, matching the TIRE-current row). The relative comparison across T_{warm} fractions is internally consistent.

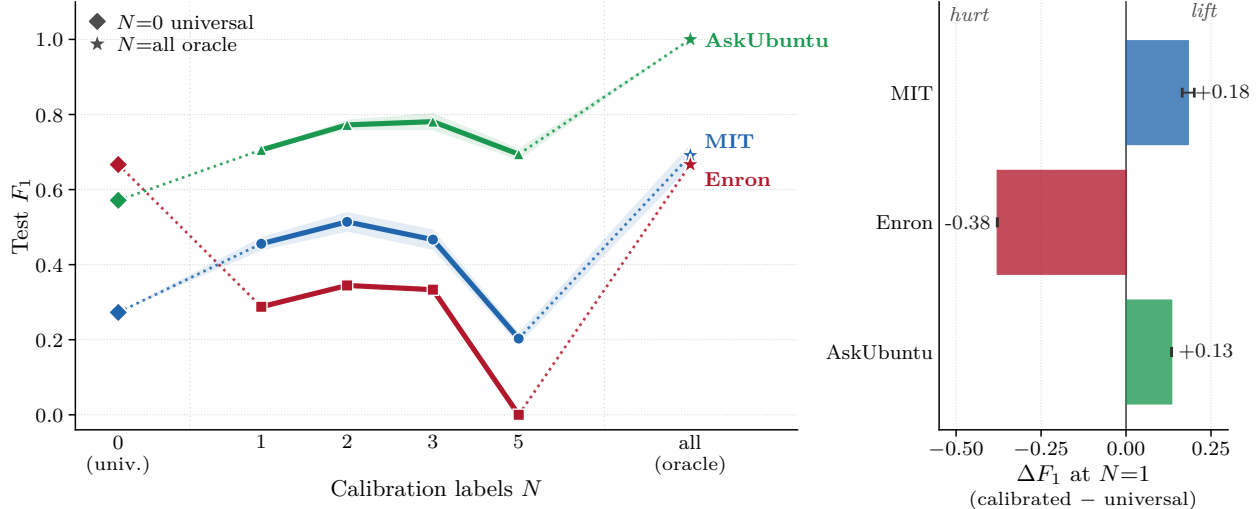


Figure 5: **Few-shot calibration with a 4-candidate pool** ($\{\text{fixed-cfg}\} \cup$ per-dataset SWORD bests). *Left*: slopegraph of test F_1 for $N \in \{0, 1, 2, 3, 5, \text{all}\}$ labeled CPs (5 stochastic seeds; shaded ± 1 std). Diamond markers anchor the $N=0$ fixed-cfg endpoint and stars anchor the $N=\text{all}$ oracle. *Right*: ΔF_1 at $N=1$ (calibrated – fixed-cfg): 1-shot *lifts* datasets where fixed-cfg is suboptimal (MIT, AskUbuntu) but *hurts* datasets where fixed-cfg is already near-optimal (Enron), reflecting calibration overfitting on a single label.

J Sensitivity to Moment Count k

Since C/k exceeds $W_1^{\max}=2$ for $k \leq 7$ (Limitation 2), we check that SWORD’s small- k regime is not a grid coincidence. Holding other hyperparameters at per-dataset best, we sweep $k \in [1, 30]$, re-tuning only the threshold at each k so that a mis-scaled threshold cannot masquerade as a k effect. Five moment-estimation seeds.

Figure 7 plots F_1 vs. k . $k = 1$ fails everywhere (a single moment is the centered eigenvalue mean). Per-dataset optima are $k = 2$ on MIT and AskUbuntu and $k = 4$ on Enron; beyond $k \approx 5$, additional moments add variance without signal. The drop is sharp on MIT and Enron (0.15–0.20) and mild on AskUbuntu (a plateau just below the peak). At each dataset’s best k the swept F_1 reproduces the headline numbers of Table 2, confirming the main grid $k \in \{2, 3, 4, 5\}$ sits on the operational plateau.

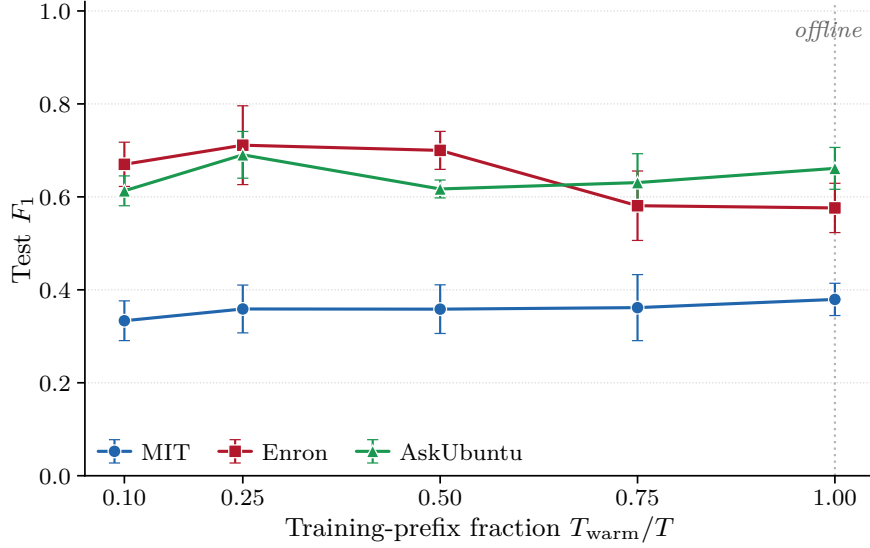


Figure 6: **TIRE under bounded online training.** Test F_1 vs. T_{warm}/T , averaged over 5 SGD seeds; error bars ± 1 std. At $T_{\text{warm}} = 0.25T$, TIRE on Enron and AskUbuntu matches or exceeds offline TIRE ($T_{\text{warm}} = T$). Online training does not degrade TIRE’s performance.

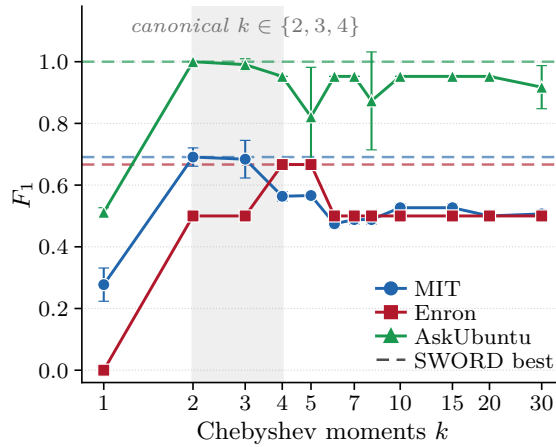


Figure 7: **Sensitivity of full SWORD to k .** For each dataset, all hyperparameters except k are held at the per-dataset best (Table 7) and the detection threshold is re-tuned at every k . Mean F_1 over 5 moment-estimation seeds; error bars are ± 1 std. Dashed line: SWORD’s per-dataset best F_1 from Table 2. The shaded band marks the $k \in [2, 4]$ regime used in the main grid.